IEEE Access
Multidisciplinary | Rapid Review | Open Access Journal

Received June 7, 2017, accepted July 23, 2017, date of publication July 27, 2017, date of current version August 14, 2017.

Digital Object Identifier 10.1109/ACCESS.2017.2732683

Duty Ratio Modulation Strategy to Minimize Torque and Flux Linkage Ripples in IPMSM DTC Systems

TIANQING YUAN[1], DAZHI WANG[1], XINGHUA WANG[2], XINGYU WANG[1], YUNLU LI[3], XIAOMING YAN[1], SEN TAN[1], AND SHUAI ZHOU[1]

[1]School of Information Science and Engineering, Northeastern University, Shenyang 110819, China
[2]Physical Education Department, School of Humanities & Law, Northeastern University, Shenyang 110819, China
[3]School of Electrical Engineering, Shenyang University of Technology, Shenyang 110027, China

Corresponding author: Tianqing Yuan (tqyuan@stumail.neu.edu.cn)

This work was supported by the National Natural Science Foundation of China under Grant 61433004 and Grant 51467017.

ABSTRACT The active vector effects on torque and flux linkage are different in interior permanent magnet synchronous motor (IPMSM) systems at different times under direct torque control (DTC). These different effects may cause overcompensation or undercompensation to torque and flux linkage leading to large torque and flux linkage ripples in the IPMSM DTC systems. A novel duty ratio modulation strategy for the IPMSM DTC systems is presented, which considers these differences that are ignored in conventional duty ratio modulation strategies. The proposed duty ratio modulation strategy aims at minimizing torque ripple and flux linkage ripple, which makes sure that the control system can work in an optimum state. The active angle, the impact angle, the active factor, and the impact factor are first introduced. The active angel and the impact angle are used to get the active factor and the impact factor, respectively. Every sector is divided into five small sectors based on the impact angels, and then, a switching table is redesigned according to the small sectors division. Also, the vector selection rules for the redesigned switching table are described in details. Subsequently, an optimal duty ratio can be derived through the simplified duty ratio determination method. Finally, the effectiveness of the proposed novel modulation strategy is verified through the experimental results on a 100-W IPMSM drive system.

INDEX TERMS Direct torque control (DTC), interior permanent magnet synchronous motor (IPMSM), torque and flux linkage ripples, duty ratio modulation strategy.

I. INTRODUCTION

Interior permanent magnet synchronous motors (IPMSM) have a lot of merits such as high reliability, high efficiency, simple construction, and good control performance, thus, it has been applied in various control systems including electrical drives, industrial implications, and medical devices in recent years [1]–[3]. The normal operations of an IPMSM need the support of high-performance control strategies. Field-oriented control (FOC) and direct torque control (DTC) are two well-established control strategies for the IPMSM. Compared to FOC, DTC aims at compensating the ripples of torque and flux linkage with eight space voltage vectors directly supplied by a two-level inverter [4]–[6]. Due to the simple structure, i.e., no current regulators or rotary coordinate transformation blocks needed, DTC can supply extremely high dynamic response for the IPMSM system.

Although the IPMSM system can obtain the needed quick dynamic response under DTC, but there still exist some problems, i.e., significant torque ripple and flux linkage ripple. Many researchers have attempted to reduce these ripples through different schemes. Space vector modulation (SVM) and duty ratio modulation are two most popular schemes that have been accepted widely. In SVM-DTC, the direction and the value of the required vector are obtained through the errors in torque and flux linkage. SVM-DTC can compensate these errors accurately with fixed switching frequency through space voltage modulate strategy, instead of the limited direction and value of the voltage vectors in conventional DTC. Varieties of methods are used to apply this strategy. In [7], feedback linearization is first introduced into SVM which can noticeably reduce torque ripple and flux linkage ripple for the interior permanent magnet synchronous

motor drives. In [8], a simple control structure for SVM-DTC including a sliding mode controller is presented, which could improve the dynamic response of the IPMSM DTC system. In [9], a quasi sliding mode observer is utilized to get the vector commands by the torque error and the flux linkage error for the control system. In [10], two resonant controllers are suggested for SVM to reduce the torque ripple. In [11], a simple proportional-integral (PI) regulator is suggested for SVM to reduce the torque ripple. Although the torque and flux linkage ripples can be reduced effectively based on these methods, but complex computations or rotary coordinate transformations are often needed, which would weaken its fast dynamic response in conventional DTC.

Another modified strategy is duty ratio modulation for DTC (DDTC). As we all know, the error values in the IPMSM are small actually in most cases. In the conventional DTC (CDTC), the active vector selections depend on the errors' characteristics in torque and flux linkage, and then the selected active vector is applied to the control system for a whole control period. The compensations to torque and flux linkage provided by the active vector are different in different period, that results leading to over-compensation or under-compensation to torque and flux linkage. In order to solve these problems, duty ratio modulation is an efficiency strategy that has been accepted widely. Duty ratio modulation strategy could maintain the fast dynamic response performance in CDTC without any complex calculations. The main goal of DDTC is to regulate the applied time of the active vector in one period. In [12], a unified switching table with the select three vectors is suggested to the novel duty ratio control scheme, this method can obtain lower flux ripple and more sinusoidal stator current. A simple and effective duty ratio regulator is obtained by considering the effects of machine angular velocity in [13]. An adaptive saturation controller is used in the novel duty ratio modulation method in [14]. However, the differences between the effect compensations to torque and of flux linkage are not considered in these strategies. This fact cannot ensure an appropriate active vector selection or an optimal duty ratio determination for the IPMSM DTC system.

Therefore, a novel duty ratio modulation strategy for the IPMSM DTC system to minimize both the torque ripple and the flux linkage ripple is proposed in this paper. To apply the proposed modulation strategy, the active angel and the impact angle are first introduced. The active factors and the impact factors to torque and flux linkage provided by the active vector are analyzed detailed. Next, a switching table based on the active factors is redesigned. Then, the rules for the active vector selection from the redesigned switching table are described. Finally, a simplified duty ratio determination method is derived. The effectiveness of the proposed novel duty ratio modulation strategy is validated through experimental results.

The organization of this paper comprises the following sections. The principle of the conventional DTC is presented in Section II. The ripples of torque and flux linkage in an IPMSM are analyzed in Section III. A novel duty ratio modulation strategy is presented in Section IV. Description of experimental setup and discussions on experimental results are given in Section V. The conclusion is detailed in section VI.

II. PRINCIPLE OF THE CONVENTIONAL DTC

There exist eight vectors V_n in the switching table which can be used in the IPMSM DTC system, including six active vectors ($V_1 \sim V_6$) and two null vectors (V_0 and V_7), as shown in the stationary $\alpha\beta$-reference frames in Fig. 1. The stator flux linkage φ_s rotation space can be divided into six sectors through six section boundary lines $l_i (i = 1, 2, 3, 4, 5, 6)$. The six sectors are represented with "N". The sector vector V_s is defined as the active vector in six sectors which φ_s located in.

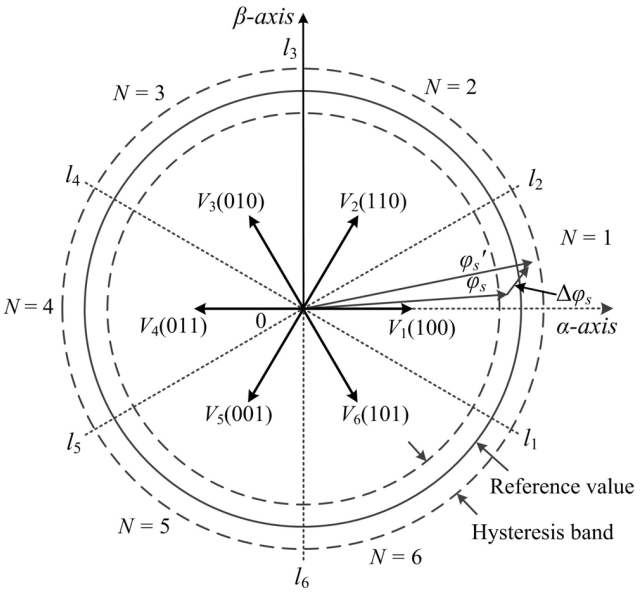

FIGURE 1. Active vector effects on the stator flux linkage.

The reference values of torque and flux linkage are T^* and φ^*, respectively, which are settled according to the parameters of the IPMSM. The hysteresis bands of torque and flux linkage are $e_i^*(i = T \text{ or } F)$, which are used for the control accuracy settings. The real-time torque T and flux linkage φ change along the reference values within the hysteresis bands. The torque error e_T and the flux linkage error e_F are obtained through the comparison between the reference values and the values of torque and flux linkage, respectively. The hysteresis controllers output the property ε_T and ε_F according to e_T and e_F.

The active vector selection rules are described in table 1. The appropriate active vector V_n will be selected depending on the property ε_T and ε_F and the sector number $N(1 \sim 6)$. And then V_n will be applied to the control system for a whole control period T_s time.

As shown in Fig. 1, the sector number is 1, the sector vector is V_1. If ε_T and ε_F are both positive, the active vector V_2 will

TABLE 1. Conventional switching table.

Sector number N		Torque	
		↑	↓
Stator flux linkage	↑	V_{N+1}	V_{N-1}
	↓	V_{N+2}	V_{N-2}

be selected and applied for the next control period T_s time. During T_s time, the effect compensation to stator flux linkage provided by V_2 is $\Delta\varphi_s$. The stator flux linkage changes from φ_s to φ_s' after this control period.

III. RIPPLES ANALYSIS IN IPMSM

The rotor permanent flux linkage φ_f is aligned with *d-axis*, the sector vector V_s is aligned with *α-axis* as shown in Fig. 2. θ_r is the angle between φ_f and *α-axis*. θ_r is the angle between φ_f and *α-axis*. θ_s is the load angle between the stator flux linkage and φ_f. θ is the active angle between the selected active vector V_n and the stator flux linkage. δ is the impact angle between the stator flux linkage and the sector vector V_s.

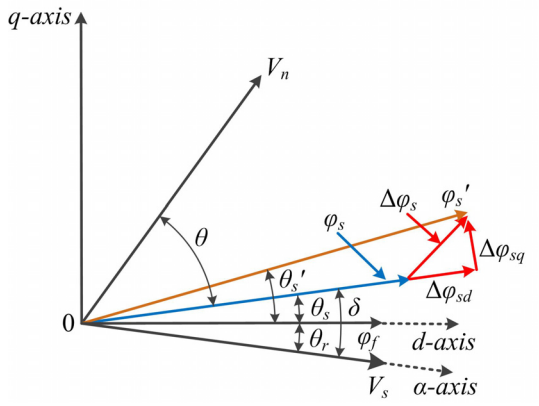

FIGURE 2. Active vector effects on torque and stator flux linkage.

It is well know that, the direction of $\Delta\varphi_s$ in any control period is the same with the applied active vector V_n in the IPMSM. The relationship between them should be

$$\Delta\varphi_s = V_n \cdot T_s \tag{1}$$

A. EFFECTS ON TORQUE AND FLUX LINKAGE PROVIDED BY THE ACTIVE VECTOR

The effect compensation of stator flux linkage $\Delta\varphi_s$ can be divided as the torque compensation $\Delta\varphi_{sq}$ and the flux linkage amplified compensation $\Delta\varphi_{sd}$. The relationships between them are given as

$$\Delta\varphi_{sq} = \Delta\varphi_s \cdot \sin\theta = V_n \cdot T_s \cdot \sin\theta \tag{2}$$
$$\Delta\varphi_{sd} = \Delta\varphi_s \cdot \cos\theta = V_n \cdot T_s \cdot \cos\theta \tag{3}$$

For the IPMSM, the rotor flux linkage amplitude is an unchangeable value, the torque value T only relate to the amplified of φ_s and the load angle θ_s. The torque value T in the IPMSM is

$$T = \frac{3p}{2L_s} \cdot \varphi_f \cdot \varphi_s \cdot \sin\theta_s \tag{4}$$

where p is the number of pole pairs, L_s is the stator inductance (H).

As the change of θ_s is nearly equal to zero [13], the variation of θ_s can be ignored, the torque compensation e_T' and the flux linkage compensation e_F' can be expressed as

$$e_T' = \frac{3p}{2L_s} \cdot \varphi_f \cdot \Delta\varphi_{sq} = \frac{3p}{2L_s} \cdot \varphi_f \cdot V_n \cdot T_s \cdot \sin\theta \tag{5}$$
$$e_F' = \Delta\varphi_{sq} = V_n \cdot T_s \cdot \cos\theta \tag{6}$$

As above analysis, if the impact angle δ is rather small, then the active angle θ is relatively big as shown in Fig. 2. The active vector effect on torque is weaker than the effect on flux linkage amplified, so e_T' is much smaller than e_F'. If e_T is small and e_F is large, it can be find that the sector vector V_1 is the most appropriate vector that should be applied, while the active vector V_2 will still be selected from table 1.

The torque will be overcompensated and the flux linkage error compensation value will not reach to the ideal point if V_2 is applied. It could see that, there exist the possibilities of an error vector selection in the conventional switching table.

B. CONVENTIONAL DUTY RATIO DETERMINATION METHOD

The stator flux linkage φ_s is located in the first sector in the stationary $\alpha\beta$-reference frame as shown in Fig. 3. If φ_s is nearly to the sector boundary line l_1, the impact angle δ is nearly equal to $-30°$. The selected active vector is V_2, so the active angle θ is nearly equal to 90°.

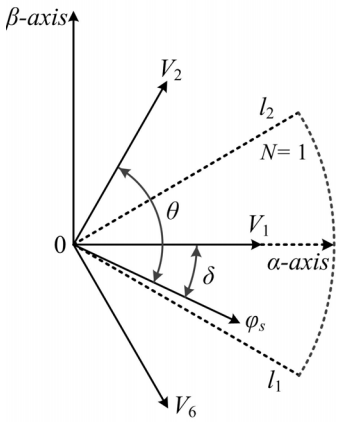

FIGURE 3. Voltage vector and stator flux linkage in the $\alpha\beta$ reference frame.

There exist significant trends of the linear correlation ship between torque compensation e_T' and flux compensation e_F'. Defined the compensation gains of e_T and e_F provided by e_T' and e_F' are k_T and k_F, respectively. The relationships among

the parameters should be

$$e'_T = \frac{3p}{2L_s} \cdot \varphi_f \cdot V_n \cdot T_s \cdot \sin\theta = k_T \cdot e_T \tag{7}$$

$$e'_F = V_n \cdot T_s \cdot \cos\theta = k_F \cdot e_F \tag{8}$$

As the active angle θ is nearly equal to 90°, it could find that the active vector effect on torque is much bigger than the effect on flux linkage, that also means k_T is much bigger than k_F. The torque duty ratio d_T and the flux linkage duty ratio d_F are given as

$$d_T = \frac{e_T}{e'_T} = \frac{e_T}{k_T \cdot e_T} = \frac{1}{k_T} \tag{9}$$

$$d_F = \frac{e_F}{e'_F} = \frac{e_F}{k_F \cdot e_F} = \frac{1}{k_F} \tag{10}$$

As k_F is rarely small, d_F may be bigger than 1. d_F should be set as 1 if its value exceed 1 due to the range of duty ratio is 0 to 1. The same setting is also applied to d_T.

In conventional duty ratio modulation strategies, the torque ripple and the flux linkage ripple are reduced without any different treat [13]–[15], or one of them is viewed as the unimportant parameter that is ignored [12]. The final duty ratio d is calculated as

$$d = \frac{d_T + d_F}{2} = \begin{cases} \dfrac{1}{2k_F}, & 0 \le d_T < d_F \le 1 \\ \dfrac{1+k_T}{2k_T}, & 0 \le d_T \le 1 < d_F \\ 1, & 1 < d_T < d_F \end{cases} \tag{11}$$

In the case "$0 \le d_T < d_F \le 1$", the torque compensation e'_{T1} and the flux linkage compensation e'_{F1} are

$$e'_{T1} = d \cdot e'_T = \frac{1}{2k_F} \cdot k_T \cdot e_T = \frac{k_T}{2k_F} \cdot e_T \gg e_T \tag{12}$$

$$e'_{F1} = d \cdot e'_F = \frac{1}{2k_F} \cdot k_F \cdot e_F = \frac{1}{2} \cdot e_F < e_F \tag{13}$$

From above calculation results, it is easy to find that the torque is overcompensated and the torque error property will exchange form positive to negative, while the compensation to flux linkage is much less than needed. The main reason is that the compensation rates to torque and flux linkage are different which provided by the active vector when the active angle θ is nearly equal to 90°.

Through above analysis, it can be seen that the active vector effects on torque and flux linkage will change with the variation of the active angle θ and the impact angle δ in the IPMSM system. This element will be considered into the novel duty ratio modulation, which is ignored in the previous duty ratio modulation methods.

IV. NOVEL DUTY RATIO MODULATION STRATEGY

To eliminate the possibility of the error vector selections and also preserve the good merits in CDTC maximally, a novel duty ratio modulation strategy is proposed as shown in Fig. 4.

In the novel modulation strategy, the differences of the active vector effects on torque and flux linkage caused by the variation of active angel θ and impact angle δ are considered. The different effects are represented by active factors μ_i (μ_T and μ_F) and impact factors λ_i(λ_T and λ_F). The calculations for μ_i and λ_i will be expressed detailed in the following parts.

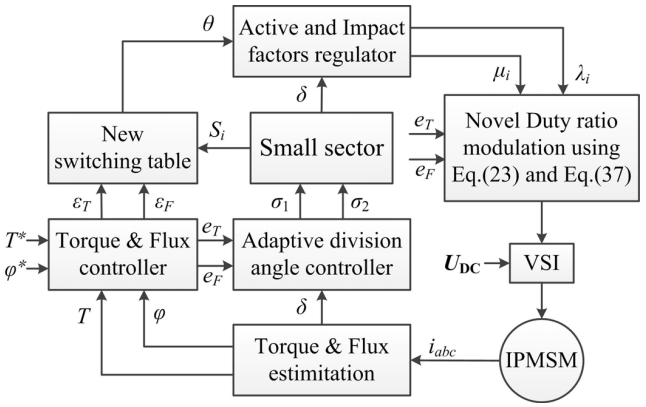

FIGURE 4. Schematic diagram of the proposed duty ratio modulation strategy.

To carry out the novel duty ratio determination method, the values of d_T and d_F are needed. In this section, the precise values of d_T and d_F will be obtained through a designed active factors regulators. And the final duty ratio d for the control system will be obtained through the impact factors regulators.

A. SMALL SECTOR DIVISION

In every sector, the impact angle δ changes from $-30°$ to 30°. We can learn from the above analysis that the active vector effects on torque and flux linkage will change with the altering of δ. The variation range of δ can be divided into five small sectors $S_i(S_0, S_{1+}, S_{1-}, S_{2+}, S_{2-})$ through the division angle σ_1 and σ_2 as shown in Fig. 5.

S_i can be divided as three kinds: S_0, S_{1+}/S_{1-}, and S_{2+}/S_{2-}, which are described through the color section yellow, blue, and grown, respectively.

1) S_0: This indicates that the stator flux linkage is nearly to the sector vector V_s. The range of δ in S_0 is

$$\delta \subset (-\sigma_1, \sigma_1) \tag{14}$$

2) S_{1+}/S_{1-}: This indicates that the stator flux linkage is in the center sector between V_s and the section boundary line l_i or l_{i+1}. The range δ in S_{1+}/S_{1-} is

$$\delta = \begin{cases} (\sigma_1\ ,\ 30° - \sigma_2)\ , & S_{1+} \\ (-30° + \sigma_2, -\sigma_1)\ , & S_{1-} \end{cases} \tag{15}$$

3) S_{2+}/S_{2-}: This indicates that the stator flux linkage is nearly to the section boundary line l_i or l_{i+1}. The range of δ in S_{2+}/S_{2-} is

$$\delta = \begin{cases} (30° - \sigma_2\ ,\ 30°)\ , & S_{2+} \\ (\text{-}30°\ ,\ \text{-}30°{+}\sigma_2)\ , & S_{2-} \end{cases} \tag{16}$$

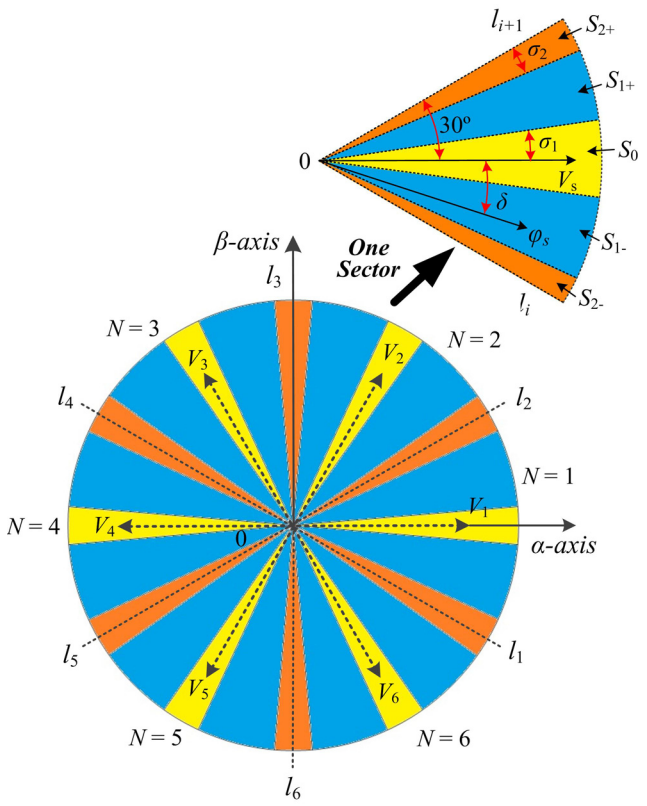

FIGURE 5. Voltage vectors and stator flux linkage in the $\alpha\beta$ reference frame and small sector division Fig. 5.

B. REDESIGNED SWITCHING TABLE AND RULES FOR ACTIVE VECTOR SELECTION

To carry out the novel duty ratio modulation strategy, the switching table in CDTC is redesigned as shown in table 2. The redesigned switching table selects the active vector with the considerations of highest efficiency of the active vector effect compensations. The active vector selection rules in table 2 are described in the following three scenarios:

1) S_0: The vector effects on torque can be divided as two situations: the effects caused by the sector vector and its opposite vector are really small, while the effects caused by the other active vectors are in the normal range. The vector effects on flux linkage can also be divided as two situations: the effects caused by the sector vector and its opposite vector are really big, while the effects caused by the other active vectors are also in the normal range. Consider the active vector effect efficiency, the flux linkage should be compensated using the sector vector or its opposite vector firstly.

2) S_{1+}/S_{1-}: The vector effects on torque and flux linkage are relatively equal, the compensation of torque and flux linkage should consider their errors comprehensively.

3) S_{2+}/S_{2-}: The vector effects on torque can be divided as two situations: the effects caused by the neighboring vectors and its opposite vectors are in the normal range, while the effects caused by the rest active vectors are really big. The vector effects on flux linkage can also be divided as two situations: the effects caused by the neighboring vectors and its opposite vector are in the normal range, while effect caused by the rest active vectors are really small. Consider the active vector effect efficiency, the torque should be compensated using the un-neighboring vector firstly.

Compared with table 1, rule (1) and (3) are added in table 2, which ensures all situations of e_T and e_F are considered, avoiding the possibility to choose an error vector.

TABLE 2. Redesigned switching table.

Small Sector			Sector number (N)
S_0		↑ (F)	V_N
		↓ (F)	V_{N+3}
S_{1+} / S_{1-}	↑ (T)	↑ (F)	V_{N+1}
		↓ (F)	V_{N+2}
	↓ (T)	↑ (F)	V_{N+5}
		↓ (F)	V_{N+4}
S_{2+}		↑ (T)	V_{N+2}
		↓ (T)	V_{N+5}
S_{2-}		↑ (T)	V_{N+1}
		↓ (T)	V_{N+4}

C. DIVISION ANGLE CONTROLLER

σ_1^* and σ_2^* are the reference values of the division angles. Define the error rates of torque and flux linkage are E_T and E_F, respectively. The division angle controller will adjust σ_1 and σ_2 based on the input of e_T and e_F through the proposed division angle controller as shown in Fig. 6.

$$\begin{bmatrix}\sigma_1\\ \sigma_2\end{bmatrix} = \begin{bmatrix}k_F & \\ & k_T\end{bmatrix} E + \begin{bmatrix}\sigma_1^*\\ \sigma_2^*\end{bmatrix} \tag{17}$$

where

$$E = \begin{bmatrix}E_F\\ E_T\end{bmatrix} = \begin{bmatrix}f_F & \\ & f_T\end{bmatrix}\begin{bmatrix}e_F\\ e_T\end{bmatrix} - \begin{bmatrix}g_F & \\ & g_T\end{bmatrix}\begin{bmatrix}\sigma_2\\ \sigma_1\end{bmatrix} \tag{18}$$

and k_T, k_F, f_T, f_F, g_T, and g_F are the constant gains that are settled according to the parameters in the IPMSM.

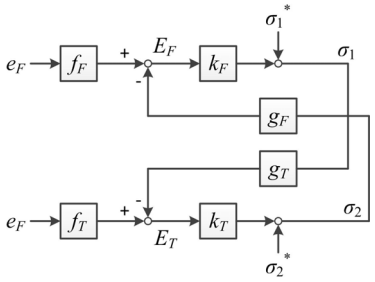

FIGURE 6. Structure of the proposed division angle controller.

If E_T is much bigger than E_F, this means the torque needs to be increased much more, the active vectors which can

increase torque quickly should be applied, that also means S_{2+} and S_{2-} should be expanded. While if E_F is bigger than E_T, this means the flux linkage needs to increase more than the torque, so the active vectors which can increase flux linkage quickly should be applied, that also means S_0 should be expanded.

D. CALCULATIONS FOR IMPACT FACTORS

Define λ^* as the evaluate value of the torque impact factor λ_T and the flux linkage λ_F. The evaluate value λ^* is obtained through a saturation controller. The saturation controller outputs not only a discrete state 0 or 1, but also the continuous value between 0 and 1. This function will make sure the precise estimate for λ^*.

Define the input value x of the saturation controller as

$$x = |\delta| - 15^\circ \tag{19}$$

The evaluate value λ^* is defined in the normalized form through the saturation controller as

$$sat\,(x, B_i) = \begin{cases} 0.5 \times (sgn\,(x) + 1)\,, & |x| \geq B_w \\ 0.5 \times (x/B_w + 1)\,, & |x| < B_w \end{cases} \tag{20}$$

where B_w is the upper boundary, and $sgn(\cdot)$ is the sign function. If x exceeds the upper boundary B_w, the saturation controller will only output the discrete state 0 or 1. However, when x is within the boundary, the input will be scaled down linearly in the range of [0, 1] at the output τ of the saturation controller. Therefore, the evaluate value between the torque impact factor and the flux linkage impact factor can be expressed as

$$\lambda^* = \begin{cases} 0, & S_0 \\ 1, & S_{2+}/S_{2-} \\ \tau, & S_{1+}/S_{1-} \end{cases} \tag{21}$$

From the relationship between the impact factors of torque and flux linkage and the evaluate value λ^*, the values of the impact factors are given as

$$\lambda_i = \begin{cases} \lambda^*, & i = T \\ 1 - \lambda^*, & i = F \end{cases} \tag{22}$$

E. SIMPLIFIED DUTY RATIO DETERMINATION METHOD

In this paper, the application of the duty ratio control method in [14] and [16] has been extended to the IPMSM. And the calculations have also been modified for the novel duty ratio modulation strategy.

The compensations to torque and flux linkage are viewed as the same provided by every active vector in [14] and [16]. However, it is well know that the compensations e'_T and e'_F will change with the variation of the active angle θ from (5) and (6), that also means the compensations to torque and flux linkage are different provided by different active vectors. Therefore, these differences that related to the active angle θ are considered into the novel duty ratio determination method to obtain an optimum duty ratio.

Define the active factors of torque and flux linkage are μ_T and μ_F, respectively. The torque duty ratio d_F and the flux linkage duty ratio d_λ in [14] and [16] can be rewritten as

$$\begin{cases} d_T = \frac{|e_T|}{C_T \cdot |\mu_T|} \\ d_F = \frac{|e_F|}{C_F \cdot |\mu_F|} \end{cases} \tag{23}$$

where e_T and e_F are the torque error and the flux linkage error, respectively. C_T and C_F are constant gains for the active vector.

In [16], the main limitations of the duty ratio are the tuning of the gains C_T and C_F. The values of C_T and C_F can be obtained through the experimentations. In this paper, the active factors of torque and flux linkage are also considered into the calculations for the duty ratio, so the values of C_T and C_F will be obtained based on the setting value of μ_T and μ_F and the experimentation.

1) Calculation for active factors: The active factors in the five small sectors can be obtained from table 2 and the active vector effect compensations in Fig. 5.

In S_0, S_{2+}, and S_{2-}, the value of μ_T and μ_F are set as

$$|\mu_T| = \begin{cases} 0, & S_i = S_0 \\ 1, & S_i = S_{2+} \\ 1, & S_i = S_{2-} \end{cases} \tag{24}$$

$$|\mu_F| = \begin{cases} 1, & S_i = S_0 \\ 0, & S_i = S_{2+} \\ 0, & S_i = S_{2-} \end{cases} \tag{25}$$

The maximum and minimum values of the active factors are 1 and 0, respectively. In S_{1+}/S_{1-}, μ_T and μ_F are variation values, the range of μ_T and μ_F will be within the limits of 0 to 1. μ_T and μ_F can be expressed through the active angle θ as

$$\mu_T = |\sin\theta| \tag{26}$$

$$\mu_F = |\cos\theta| \tag{27}$$

The ranges of μ_T and μ_F in S_{1+}/S_{1-} are

$$\Delta\mu_i = \begin{cases} (0.5, 1)\,, & \text{i=T} \\ (0, 0.9)\,, & \text{i=F} \end{cases} \tag{28}$$

Through linearization theory, the calculations for the values of μ_T and μ_F with different active angle θ are given as

$$\begin{cases} \mu_T = \mu_1 + k_1 \cdot |\theta|\,, & |\theta| \subset (30^\circ, 90^\circ) \\ \mu_T = \mu_2 + k_2 \cdot |\theta|\,, & |\theta| \subset [90^\circ, 150^\circ) \\ \mu_F = \mu_3 + k_3 \cdot |\theta|\,, & |\theta| \subset (30^\circ, 150^\circ) \end{cases} \tag{29}$$

where μ_1, μ_2, and μ_3 are the initial point values that chosen as 0.25, 1.75, and 1.35, respectively. And k_1, k_2, and k_3 are the change rates, the value of them are 0.008, -0.008, and -0.015, respectively.

2) Calculations for final duty ratio: To obtain the best operation of the control system, both torque ripple and flux linkage ripple need to be reduced. In order to simply the

calculation of the final duty ratio d, the ripple rates with the compensations provided by the active vector are rewritten as

$$E_T^2 = \left(\frac{d \cdot e'_T - e_T}{e_T^*}\right)^2 \tag{30}$$

$$E_F^2 = \left(\frac{d \cdot e'_F - e_F}{e_F^*}\right)^2 \tag{31}$$

The compensations of torque and flux linkage in (9) and (10) can be expressed as

$$e'_T = \frac{1}{d_T} \cdot e_T \tag{32}$$

$$e'_F = \frac{1}{d_F} \cdot e_F \tag{33}$$

The ripple rates in (30) and (31) can be expressed in more detail as

$$E_T^2 = \left(\frac{d \cdot \frac{1}{d_T} \cdot e_T - e_T}{e_T^*}\right)^2 = \left(\frac{e_T}{e_T^*}\right)^2 \left(\frac{1}{d_T} \cdot d - 1\right)^2 \tag{34}$$

$$E_F^2 = \left(\frac{d \cdot \frac{1}{d_F} \cdot e_F - e_F}{e_F^*}\right)^2 = \left(\frac{e_F}{e_F^*}\right)^2 \left(\frac{1}{d_F} \cdot d - 1\right)^2 \tag{35}$$

The ripple rates E_T^2 and E_F^2 are proportional to the square of the duty ratio variable d. The final duty ratio d is a parameter that can respond the compensations for the torque ripple and the flux linkage ripple.

The torque impact factor λ_T and the flux linkage λ_F are used to determine the proportion of the ripple rates E_T^2 and E_F^2 in the synthetic ripple rate E^*.

$$E^* = (\lambda)^m \cdot E_T^2 + (1-\lambda)^m \cdot E_F^2 \tag{36}$$

To determine the value of m, the state of the IPMSM within a certain time is analyzed. The main parameters in the control system are shown in table 3.

TABLE 3. Main parameters in the IPMSM.

δ	-24.5°
θ	54.5°
N	1
e_T	$0.05N{\cdot}m$
e_F	$0.007Wb$
V_s	V_1
V_n	V_2

With the active vector applied for a whole control period, the torque compensation coefficient k_T is 3, and the flux linkage compensation coefficient k_F is 0.4. The relationships between the duty ratio d and the ripple rates are shown in Fig. 7. It could find that the minimum point of the torque ripple rate and the flux linkage ripple rate corresponding different duty ratio, and their value are 0.3 and 2.5, respectively.

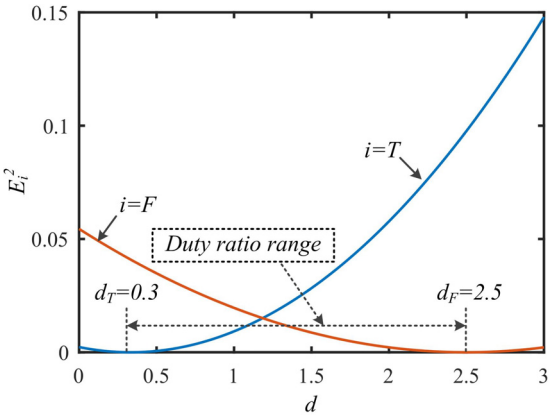

FIGURE 7. The relationships between the ripple rates of torque and flux linkage and the duty ratio.

As the range of duty ratio is 0 to 1, the optimum duty ratio should choose from 0.3 to 1. The synthetic ripple E^* with different values of m based on variations duty ratio value are analyzed as shown in Fig. 8. It could find that, the minimum ripple rate appears at the point of duty ratio is less than 0.4 with different values of m. The ripple rates will reduce significantly when m changes from 1 to 2. The variation of m will affect the ripple rate little if m is large than 2. Therefore, the best optimum value m for the novel duty ratio determination method is 2.

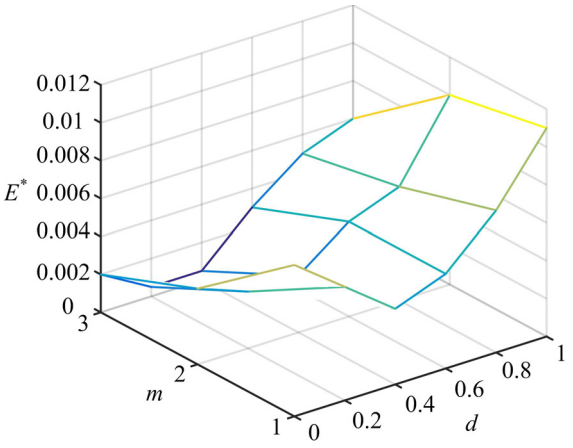

FIGURE 8. The relationships between the ripple rate and the duty ratio.

The minimum value of the synthetic ripple rate can be obtained by letting $dE^*/dd = 0$. The optimum value d is

$$d = \frac{\left(e_F^*\right)^2 \cdot e_T^2 \cdot \lambda^2 \cdot \frac{1}{d_T} + \left(e_T^*\right)^2 \cdot e_F^2 \cdot (1-\lambda)^2 \cdot \frac{1}{d_F}}{\left(e_F^*\right)^2 \cdot e_T^2 \cdot \lambda^2 \cdot \frac{1}{d_T^2} + \left(e_T^*\right)^2 \cdot e_F^2 \cdot (1-\lambda)^2 \cdot \frac{1}{d_F^2}} \tag{37}$$

V. EXPERIMENTAL ANALYSIS

A. EXPERIMENTAL SYSTEM SETUP

Experimental studies are carried out on a 100-W IPMSM drive system to validate the proposed duty ratio modulation

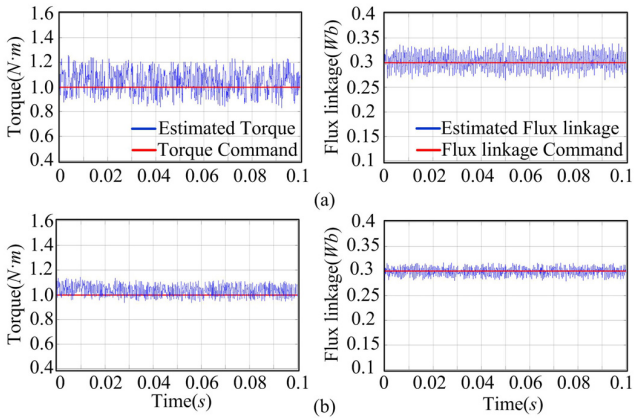

FIGURE 9. Experimental torque and flux linkage of the IPMSM at 300 *rpm* when using: (a) CDTC and (b) DDTC.

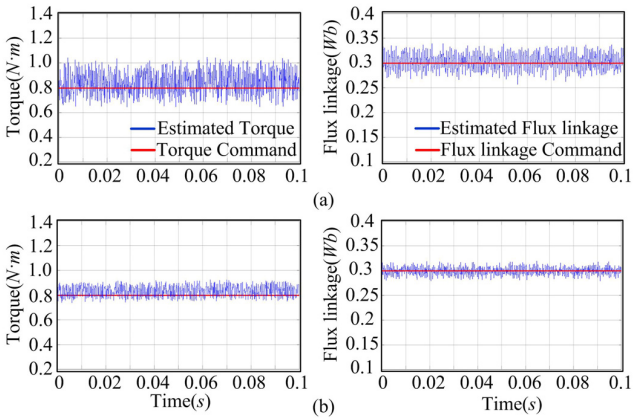

FIGURE 10. Experimental torque and flux linkage of the IPMSM at 500 *rpm* when using: (a) CDTC and (b) DDTC.

strategy. The parameters of the IPMSM are given as follows: $R_s = 1.1\ \Omega$; $L_s = 0.0085\ H$; the number of pole pairs $p = 4$. The DC voltage is 300 V. This study compares the steady-state and the dynamic performance of CDTC and DDTC. The experiments are implemented in a TMS320F28335 DSP control system with a sampling period of 100 μs. The boundaries of torque and flux linkage hysteresis comparators in two control systems are set to be 0.1 $N \cdot m$ and 0.005 Wb, respectively.

B. STEADY-STATE PERFORMANCE

The steady-state performances of CDTC and DDTC are compared under different operating conditions. First, the IPMSM is operated at 300 *rpm* and the reference values of torque and flux linkage are $1N \cdot m$ and 0.3 Wb, respectively. The torque and flux linkage waveforms of CDTC and CDTC are shown in Fig. 9. The torque ripples of CDTC and DDTC are 0.35 and 0.2 $N \cdot m$, respectively; and the flux linkage ripples of CDTC and DDTC are 0.04 and 0.025 Wb, respectively. The average torques of the IPMSM controlled by CDTC and DDTC are 1.1 and 1.05 $N \cdot m$, respectively. When the rotor speed is increased to 500 *rpm* and the torque command is changed to 0.8 $N \cdot m$, the torque ripples of CDTC and DDTC are 0.3 and $0.16N \cdot m$, respectively; and the flux linkage ripples of CDTC and DDTC are 0.05 and 0.025 Wb, respectively, as shown in Fig. 10. The average torques of the IPMSM controlled by CDTC and DDTC are 0.85 and 0.82 $N \cdot m$, respectively. From these results it can be seen that, compared with CDTC, DDTC can reduce the torque ripple by at least 42%, and reduce the flux linkage ripple at least 37%. Therefore, the proposed DDTC shows superiority over CDTC in reducing the steady-state torque and flux linkage ripples under different operating conditions. Furthermore, the average torque using DDTC and the torque command are on top of each other, thus fully eliminating the steady-state torque tracking error present in CDTC.

C. DYNAMIC PERFORMANCE

To validate the fast dynamic response of the novel duty ratio modulation strategy, the torque command is changed from 0 to 1 $N \cdot m$ at 0.1 ms when the rotor speed is 400 *rpm*. The dynamic responses of CDTC and DDTC are compared in Fig. 11. When DDTC is used, the torque increases from 0.02 to 1 $N \cdot m$ within 0.02 s. In the same period, CDCT increases the torque from -0.01 to 1 $N \cdot m$. The results show that the response time of DDTC are similar to that of CDTC. Therefore, the main advantage of CDTC, i.e., the fast dynamic response, is retained in DDTC.

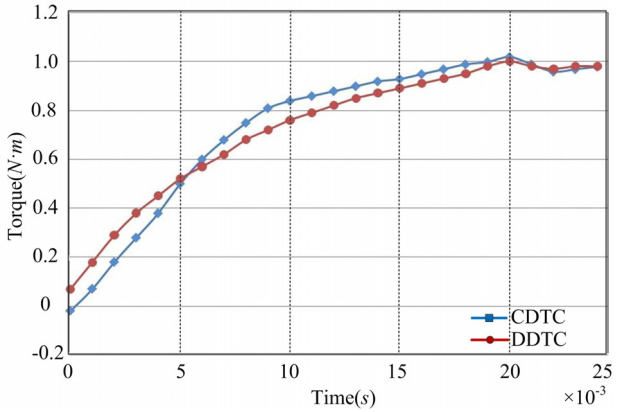

FIGURE 11. Comparison of transient responses of CDTC and DDTC.

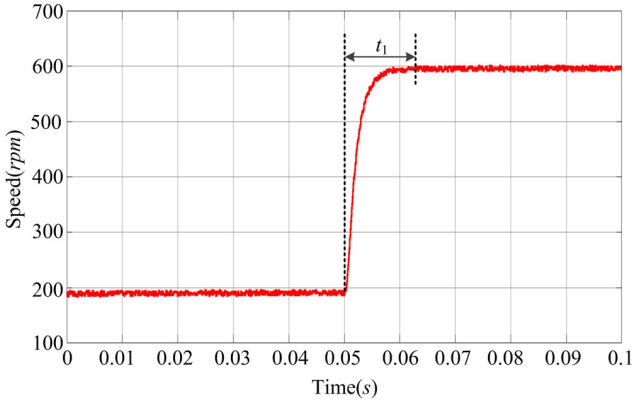

FIGURE 12. The speed trajectory from 200 *rpm* to 600 *rpm* using CDTC.

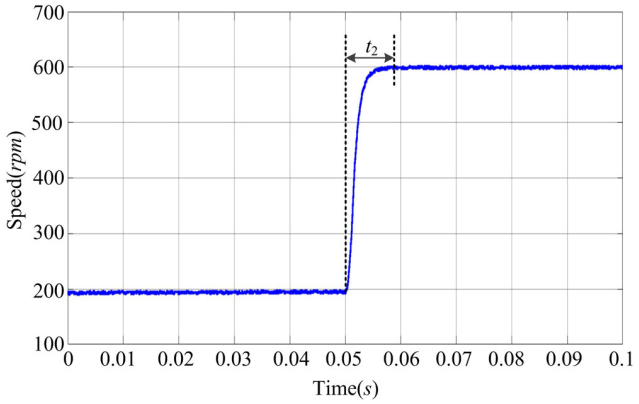

FIGURE 13. The speed trajectory from 200 *rpm* to 600 *rpm* using DDTC.

The dynamic speed responses of CDTC and DDTC are also tested. In these tests, Firstly, a step change from 200 to 600 *rpm* is applied on the speed reference at 0.05 *s*, as shown in Fig. 12, and 13. It can be seen that by using the proposed DDTC, the ripples of the rotor speed are less than 9 *rpm*. However, when using CDTC, the speed ripples have reached 15 *rpm*. Moreover, since DDCT can generate a larger mean torque than CDTC, the settle down time of the rotor speed t_1 using DDCT is approximately 0.0085 *s*, which is 0.0035 *s* faster than CDTC. Therefore, the merit of fast dynamic response of CDTC is preserved by DDTC while achieving reduced torque and flux linkage ripples.

VI. CONCLUSION

This paper proposes a novel approach for the calculations of duty ratio for the IPMSM DTC systems. To calculate the ripples in torque and flux linkage accurately and easily, the impact factors and the active factors of torque and flux linkage are considered. The active vector can be selected preciously and the exact duty ratio can be obtained easily. The torque and flux linkage ripples are evaluated comprehensively to calculate the precise duty ratio for the IPMSM DTC system, so the minimum ripples of torque and flux linkage can be obtained.

Experimental results clearly indicate that the novel duty ratio scheme exhibits excellent control of torque and flux linkage with lower steady-state ripples, and faster transient response performance when compared to the conventional DTC.

REFERENCES

[1] G. S. Buja and M. P. Kazmierlowski, "Direct torque control of PWM inverter-fed AC motors—A survey," *IEEE Trans. Ind. Electron.*, vol. 51, no. 4, pp. 744–757, Aug. 2004.

[2] A. K. Putri, S. Rick, D. Franck, and K. Hameyer, "Application of sinusoidal field pole in a permanent-magnet synchronous machine to improve the NVH behavior considering the MTPA and MTPV operation area," *IEEE Trans. Ind. Appl.*, vol. 52, no. 3, pp. 2280–2288, May/Jun. 2016.

[3] M. Lebmann, T. Finocchiaro, U. Steinseifer, T. Schmitz-Rode, and K. Hameyer, "Concepts and designs of life support systems," *IET Sci., Meas. Technol.*, vol. 2, no. 6, pp. 499–505, Nov. 2008.

[4] C. Lascu and A. M. Trzynadlowski, "Combining the principles of sliding mode, direct torque control, and space-vector modulation in a high-performance sensorless AC drive," *IEEE Trans. Ind. Appl.*, vol. 40, no. 1, pp. 170–177, Jan./Feb. 2004.

[5] F. Niu, B. Wang, A. S. Babel, K. Li, and E. G. Strangas, "Comparative evaluation of direct torque control strategies for permanent magnet synchronous machines," *IEEE Trans. Power Electron.*, vol. 31, no. 2, pp. 1408–1424, Feb. 2016.

[6] A. Tripathi, A. M. Khambadkone, and S. K. Panda, "Torque ripple analysis and dynamic performance of a space vector modulation based control method for AC-drives," *IEEE Trans. Power Electron.*, vol. 20, no. 2, pp. 485–492, Mar. 2005.

[7] Y.-S. Choi, H. H. Choi, and J.-W. Jung, "Feedback linearization direct torque control with reduced torque and flux ripples for IPMSM drives," *IEEE Trans. Power Electron.*, vol. 31, no. 5, pp. 3728–3737, May 2016.

[8] Y. Zhang, J. Zhu, W. Xu, and Y. Guo, "A simple method to reduce torque ripple in direct torque-controlled permanent-magnet synchronous motor by using vectors with variable amplitude and angle," *IEEE Trans. Ind. Electron.*, vol. 58, no. 7, pp. 2848–2859, Jul. 2011.

[9] Z. Zhang, Y. Zhao, W. Qiao, and L. Qu, "A space-vector-modulated sensorless direct-torque control for direct-drive PMSG wind turbines," *IEEE Trans. Ind. Appl.*, vol. 50, no. 4, pp. 2331–2341, Jul./Aug. 2014.

[10] A. H. Abosh, Z. Q. Zhu, and Y. Ren, "Reduction of torque and flux ripples in space vector modulation-based direct torque control of asymmetric permanent magnet synchronous machine," *IEEE Trans. Power Electron.*, vol. 32, no. 4, pp. 2976–2986, Apr. 2017.

[11] L. Tang, L. Zhong, M. F. Rahman, and Y. Hu, "A novel direct torque controlled interior permanent magnet synchronous machine drive with low ripple in flux and torque and fixed switching frequency," *IEEE Trans. Power Electron.*, vol. 19, no. 2, pp. 346–354, Mar. 2004.

[12] Y. Zhang and J. Zhu, "A novel duty cycle control strategy to reduce both torque and flux ripples for DTC of permanent magnet synchronous motor drives with switching frequency reduction," *IEEE Trans. Power Electron.*, vol. 26, no. 10, pp. 3055–3067, Oct. 2011.

[13] Y. Ren, Z. Q. Zhu, and J. Liu, "Direct torque control of permanent-magnet synchronous machine drives with a simple duty ratio regulator," *IEEE Trans. Ind. Electron.*, vol. 61, no. 10, pp. 5249–5258, Oct. 2014.

[14] Z. Zhang, C. Wei, W. Qiao, and L. Qu, "Adaptive saturation controller-based direct torque control for permanent-magnet synchronous machines," *IEEE Trans. Power Electron.*, vol. 31, no. 10, pp. 7112–7122, Oct. 2016.

[15] F. Niu, K. Li, and Y. Wang, "Direct torque control for permanent-magnet synchronous machines based on duty ratio modulation," *IEEE Trans. Ind. Electron.*, vol. 62, no. 10, pp. 6160–6170, Apr. 2015.

[16] M. A. M. Cheema, J. E. Fletcher, D. Xiao, and M. F. Rahman, "A direct thrust control scheme for linear permanent magnet synchronous motor based on online duty ratio control," *IEEE Trans. Power Electron.*, vol. 31, no. 6, pp. 4416–4428, Jun. 2016.

TIANQING YUAN received the B.S. degree in electrical engineering from the Shenyang University of Technology, Shenyang, China, in 2016. He is currently pursuing the Ph.D. degree with Northeastern University, Shenyang, China.

His research interest includes permanent magnet motor drives, power electronics, and high performance control strategy.

DAZHI WANG received the B.S. degree in automation from the Southeastern University of China, Nanjing, China, in 1985, the M.S. degree in automation from the Shenyang Ligong University of China, Shenyang, China, in 1992, and the Ph.D. degree in control theory and control engineering from Northeastern University, Shenyang, in 2003.

He is currently a Full Professor and the Head of the Institute of Power System and Drives, School of Information Science and Engineering, Northeastern University. His current research interests include renewable energy generation system, power electronics, power quality control, and motor drives.

XINGHUA WANG received the B.S. degree in social sport from Beijing Sport University, Beijing, China, in 2014, and the M.S. degree in leisure and sport management from Hong Kong Baptist University, Hong Kong, in 2015. She is currently pursuing the Ph.D. degree in education economy and management with Northeastern University, Shenyang, China.

She is currently a Lecturer with the P.E. Department, Northeastern University. Her research interests include sport management, sport marketing, and public sport service.

XINGYU WANG received the B.S. degree in electrical engineering and automation and the M.S. degree in electrical engineering from Liaoning Technical University, Fuxin, China, in 2014 and 2017, respectively. He is currently pursuing the Ph.D. degree in power electronics and power drives with Northeastern University, Shenyang, China.

His research interests include sliding electrical contact and basic theory of electrical equipment.

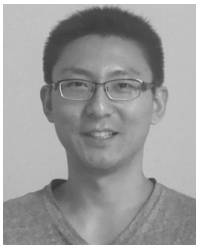

YUNLU LI received the B.S. degree in electronic information engineering from the Shenyang University of Technology, Shenyang, China, in 2009, and the M.S. degree in control engineering and the Ph.D. degree in power electronics and power drives from Northeastern University, Shenyang, China, in 2011 and 2017, respectively.

He is currently with the School of Electrical Engineering, Shenyang University of Technology. His research interests include phase-locked loop and nonlinear filtering techniques for distributed systems and power quality.

XIAOMING YAN received the B.S. degree in measurement techniques and instrumentation from Northeastern University, Shenyang, China, in 2015. He is currently pursuing the M.S. degree in control engineering with Northeastern University, China.

His current research interests include motor drives and power electronics.

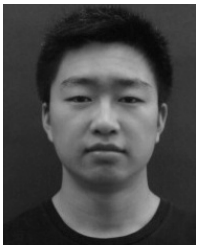

SEN TAN received the B.S. degree from Northeastern University, Shenyang, China, in 2014, where he is currently pursuing the M.S. degree in control engineering.

His current research interests include power system and power electronics, electrical machines, and their control systems.

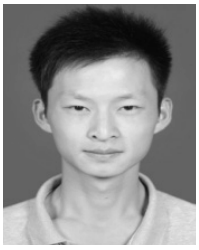

SHUAI ZHOU received the B.S. degree in electrical engineering and automation from the Shenyang University of Chemical Technology, Shenyang, China, in 2013, and the M.S. degree in control engineering from Shenyang Ligong University, Shenyang, in 2016.

His research interests include dynamics and control of modular multilevel power electronic systems and electric vehicle charging research on advanced control strategy of electric power.